Modelling of depth-induced wave breaking over sloping and horizontal beds

ANDRÉ J. VAN DER WESTHUYSEN

Deltares | Delft Hydraulics, P.O. Box 177, 2600 MH, Delft, The Netherlands

E-mail: andre.vanderwesthuysen@deltares.nl

1. Introduction

The spectral wind wave model SWAN (Booij et al. 1999) is widely used for the computation of wave fields over shelf seas, in coastal areas and in shallow lakes. The accurate estimation of wave field statistics by such models is important for various applications in these environments. SWAN computes the evolution of wave action density N ($= E/\sigma$, where E is the variance density and σ the relative radian frequency) using the action balance equation:

$$\frac{\partial N}{\partial t} + \nabla_{x,y} \cdot \left[(\mathbf{c_g} + \mathbf{U}) N \right] + \frac{\partial}{\partial \theta} (c_\theta N) + \frac{\partial}{\partial \sigma} (c_\sigma N) = \frac{S_{\text{tot}}}{\sigma} \tag{1}$$

with

$$S_{\text{tot}} = S_{\text{in}} + S_{\text{wc}} + S_{\text{nl4}} + S_{\text{bot}} + S_{\text{brk}} + S_{\text{nl3}} \tag{2}$$

The terms on the left-hand side of (1) represent, respectively, the change in wave action over time, the propagation of wave action in geographical space (with $\mathbf{c_g}$ the wave group velocity vector and $\mathbf{U}$ the ambient current), depth- and current-induced refraction (with propagation velocity c_θ in directional space θ) and the shifting of the relative radian frequency σ due to variations in mean current and depth (with the propagation velocity c_σ). The right-hand side of (1) represents processes that generate, dissipate or redistribute wave energy, given by (2). These include the deep water processes of wind input (S_{in}), whitecapping dissipation (S_{wc}), quadruplet nonlinear interaction (S_{nl4}), and the shallow water processes of bottom friction dissipation (S_{bot}), depth-induced breaking (S_{brk}) and triad nonlinear interaction (S_{nl3}).

The Dutch Wadden Sea in the north of the Netherlands is a complex coastal system that poses significant challenges to nearshore wave modelling. The region is enclosed by a series of barrier islands and the Dutch mainland coast. Tidal inlets are found between the barrier islands, each featuring an ebb tidal delta, one or more main tidal channels, and a complex system of smaller channels and flats extending into the Wadden Sea interior. Apart from the tidal channels, the Wadden Sea interior is shallow and flat, with tidally-modulated depths ranging between 0 m (dry fall)
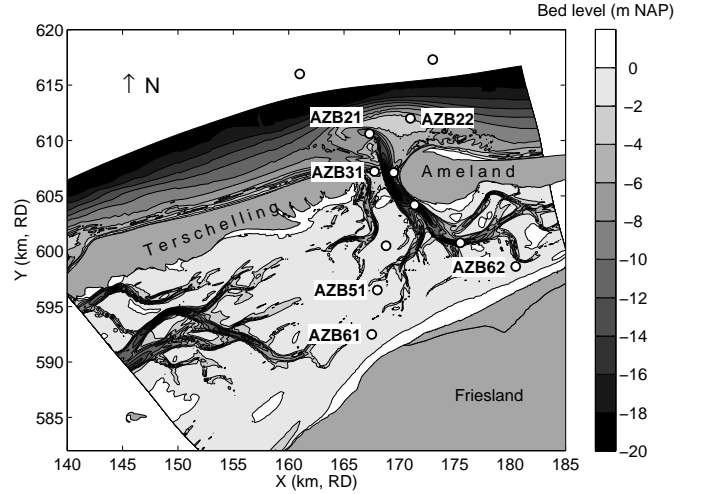
FIG. 1. Bathymetry of the Amelander Zeegat region in the Dutch Wadden Sea, including the location of the wave buoys (circles). Investigated buoy locations are labelled. Depth contours in m below NAP and projection in Dutch RD system.

and 3 m, but which can reach 6 m during extreme storms. The Amelander Zeegat tidal inlet (Figure 1) is found between the barrier islands of Terschelling (to the west) and Ameland (to the east). A program of wave monitoring has been operational in this inlet since 2003 (Zijderveld and Peters 2008). Hindcast studies based on this data (Groeneweg et al. 2008; Van Vledder et al. 2008) have shown that the ebb-tidal delta strongly shields offshore waves, so that the wave field in the Wadden Sea interior is dominated by locally-generated wind sea developing over finite depth. Moreover, it was found that SWAN typically underestimates wave heights and periods over the shallow flats. This inaccuracy can be expressed as an underestimation of the dimensionless ratio H_{m0}/d of the locally-generated wind sea, where H_{m0} is the significant wave height and d the local water depth. An upper limit of H_{m0}/d of about 0.38 is computed by SWAN, whereas observed values of as high as 0.43 are found. A number of studies for shallow Dutch lakes have shown a similar tendency for SWAN to

underestimate wave heights and periods under conditions of finite-depth wave growth over near-horizontal topography (De Waal 2002; Bottema and Beyer 2002; Bottema et al. 2002; Van der Westhuysen et al. 2007; Bottema and Van Vledder 2009). In all these studies, a consistent underprediction of higher values of the dimensionless ratio H_{m0}/d was reported. It is important that this model inaccuracy be resolved, since it greatly affects the reliability of wave estimates in these finite-depth environments.

Under storm conditions, the locally-generated waves in the Dutch Wadden Sea and shallow Dutch lakes can develop to a finite-depth wave growth limit, as described for example by Bretschneider (1958), Young and Verhagen (1996) and recently Young and Babanin (2006). These conditions are distinct from the situation where waves are generated in deep water and subsequently dissipated due to decreasing water depth (be it a monotonically sloping, barred or terraced beach) across a surf zone towards the shore.

The depth-induced breaking expression of Battjes and Janssen (1978), hereafter BJ78, that was developed for surf zone environments and used in SWAN, has proven to be successful in a wide range of situations. However, this formulation has mainly been studied for the case of waves from deeper water breaking on a beach. Its role in finite-depth wave growth has received relatively little attention. The main calibration parameter in the formulation of BJ78 is the breaker index γ_{BJ}, originally used with a constant value of 0.8. Later studies proposed dependencies of γ_{BJ} on various wave field variables (e.g., Battjes and Stive 1985; Nairn 1990; Massel and Gourlay 2000; Ruessink et al. 2003; Holthuijsen and Booij 2006; Apotsos et al. 2008).

In a recent study, Van der Westhuysen (2009), hereafter W09, investigates the role of depth-induced breaking in situations of finite-depth wave growth over near horizontal bathymetry. The BJ78 model, applied with $\gamma_{BJ} = 0.73$ (default in SWAN) was shown to be the main cause of the underprediction of wave heights, since it overestimates the breaker dissipation under these conditions. This confirmed earlier suggestions by Bottema and Beyer (2002), Bottema et al. (2002) and Bottema and van Vledder (2009). Regarding parameterizations of γ_{BJ} in the literature, that of Ruessink et al. (2003) was found to adequately yield the lower levels of depth-induced breaker dissipation found under these conditions. This result was confirmed by Zijlema (2009).

Based on this analysis, as well as earlier work by Gourlay (1994) and Massel and Gourlay (2000), W09 proposes a new estimation of the breaker index, based on the local shallow water nonlinearity. Implemented in the bore-based breaker model of Thornton and Guza (1983), the resulting formulation (the so-called biphase breaker model) accurately predicts the large difference in dissipation magnitudes found between surf zone conditions (high nonlinear-

ity) and finite-depth growth situations (low-nonlinearity). W09 noted a further dependency of the breaker data on the mean wave steepness, showing lower dissipation levels for lower wave steepness and *vice versa*, but did not include this refinement in the model. In addition, the W09 model was only verified for uni-modal spectra, whereas bi-modal spectra often occur in coastal regions. These two aspects are addressed in the present study.

The overall goal with the biphase breaker model of W09 is to improve the modelling of finite-depth wave growth, whilst retaining the good performance over sloping-bed surf zones of models such as BJ78. The aim of the present study is to refine the biphase breaker model by including a dependency of breaking intensity on the local wave steepness, and to evaluate the model for a wide range of finite-depth wave growth and sloping-bed surf zone conditions.

To achieve the study's aims, the modelling of depth-induced breaking using the biphase breaker model was studied for a data set consisting of 69 cases of laboratory and field observations. In order to ensure generality of the results, this data set features both surf zone and finite-depth wave growth situations. Section 2 presents the biphase breaker model, and the inclusion of a wave steepness dependency investigated in the present study. This section also describes the data set used and the method of evaluation used. Section 3 presents the calibration of the breaker model. Subsequently, the model performance is compared for various conditions (Section 4). Section 5 closes the paper with conclusions and a discussion.

2. Method

a. The biphase breaker model

Recently, W09 presented a new model for depth-induced breaking based on the local shallow water nonlinearity of the wave field. This model is based on earlier work by Gourlay (1994) and Massel and Gourlay (2000), and an approach for modelling of depth-induced breaking followed in phase-resolving wave models. Schäffer et al. (1993) show that in phase-resolving Boussinesq wave models, the breaking criterion can be related to the slope of the forward face of a shoaling wave. In shallow water, this forward face steepens due to triad nonlinear interaction. This suggests a correlation between the shallow water nonlinearity of waves, expressed in terms of their evolving asymmetry, and their breaking probability.

Figure 2(a) shows the relationship between the wave field asymmetry, computed by

$$A_s = \frac{\left\langle \mathrm{H}(\eta(t))^3 \right\rangle}{\left\langle \eta(t)^2 \right\rangle^{3/2}} \quad , \qquad (3)$$

and the observed fraction of breaking waves Q_b throughout the surf zone, in flume data of Boers (1996). In (3),
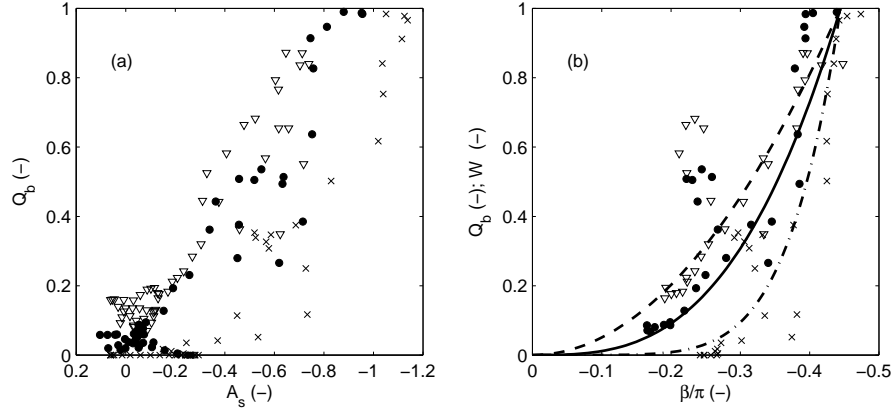
FIG. 2. Scatter plots of breaking statistics versus parameters for the wave field nonlinearity. Panel (a): Q_b versus asymmetry A_s. Panel (b): Q_b versus the biphase β. Included is parameterization (6) with $\beta_{ref} = -4\pi/9$, with exponent n varying according to (7): $n = 2$ (dashed), $n = 3$ (solid) and $n = 6$ (dash-dot). Data shown are the cases 1A (filled circles), 1B (inverted triangles) and 1C (crosses) of Boers (1996).

the operator H(.) is the Hilbert transform and $\eta(t)$ is the time series of the surface elevation. It can be seen in Figure 2(a) that a general correlation between the asymmetry A_s and Q_b appears to exist throughout the surf zone—low asymmetry corresponds to a low fraction of breakers, whereas high asymmetry corresponds to a high Q_b, and therefore intensive breaking. The data furthermore shows a dependency on the wave steepness (distinguished by different symbols). For the case with the lowest wave steepness (case 1C of Boers (1996)), a given Q_b corresponds to the highest wave asymmetry value of the three cases.

The evolution of the wave field asymmetry A_s is, however, not computed in phase-averaged wave models based only on the energy or action balance equation, such as SWAN. Another variable related to the wave shape is the biphase, the phase angle of the complex bispectrum. The biphase evolves from 0 to $-\pi/2$ through the surf zone, leading to the evolution of the wave profile from vertically symmetrical to a saw-tooth shape. As such, the biphase appears to be a suitable variable by which to approximate the asymmetry of the wave profile. Doering and Bowen (1995) and Eldeberky (1996) have proposed parameterizations for $\beta(f_p, f_p)$, the biphase of the self-interactions of the primary (spectral peak frequency), in terms of the local Ursell number. Here the parameterization of Eldeberky (1996) is used, which reads:

$$\beta(f_p, f_p) = -\frac{\pi}{2} + \frac{\pi}{2} \tanh\left(\frac{0.2}{Ur}\right) \quad , \qquad (4)$$

in which Ur is the Ursell number. The latter is defined as the ratio of the wave steepness ak to the cube of the relative depth, $(kd)^3$. Eldeberky (1996) gives the following spectral mean expression for the Ursell number:

$$Ur = \frac{g}{8\sqrt{2}\pi^2} \frac{H_{m0} T_{m01}{}^2}{d^2} \qquad (5)$$

where T_{m01} is the mean period. Based on the description above, breaking probability in the surf zone can be expected to be related to the biphase $\beta(f_p, f_p)$ (henceforth referred to as β for brevity). For $\beta = 0$, the waves are vertically symmetrical and hence should not break due to bottom influence (although they may still experience steepness-induced breaking). As $\beta \rightarrow -\pi/2$, waves become saw-toothed and break due to an unstable front face, ultimately caused, via triad interaction, by the decreasing depth. Figure 2(b) shows, by means of a scatter plot of Q_b versus β of the Boers (1996) data, that this is indeed the case. Note, however, that $Q_b \approx 1$ is reached somewhere before $\beta = -\pi/2$, namely at a biphase β of around $-4\pi/9$ (or $-80°$). For values in-between these limits, there appears to be a power law relationship between β and Q_b. An exception is found at $\beta \approx -\pi/4$, where an excursion from the power law trend is seen. In space, this corresponds to the region immediately inshore of the bar (cf. Figure 2(b)). Within this region, the magnitude of the biphase β computed using (4) and (5) is likely to be inaccurate, since it depends on local variables only, neglecting its evolution history in space. Due to the strong increase in water depth behind the bar, the magnitude of β drops here, leading to the observed excursion. However, since the bulk of breaking dissipation typically occurs on the seaward face of bars, the model will be shown to perform satisfactorily nonetheless.

Hence, it can be concluded that the observations support there being a relationship between β and the fraction of breaking waves of the general form:

$$W = \left(\frac{\beta}{\beta_{\text{ref}}} \right)^n \quad , \tag{6}$$

in which W represents the fraction of breakers, as used in the bore-based model of Thornton and Guza (1983). The denominator β_{ref} is a calibration parameter, and represents the biphase at which all waves are considered to be breaking ($Q_{\text{b}} = 1$), where $W = 1$.

As found with the wave asymmetry, Figure 2(b) shows a dependency of the relationship between Q_{b} and β on the wave steepness. The wave condition 1C, with lower steepness than the other two conditions studied by Boers (1996), reaches higher values of β before breaking. Doering and Bowen (1995) note a similar phenomenon for their data set. As an extension to the W09 model, this effect is included here by allowing the exponent n to vary with the mean local wave steepness, based on the Boers (1996) data:

$$n = \frac{n_1 + n_2}{2} - \frac{n_2 - n_1}{\pi} \arctan \left[\nu \left(S_{\text{loc}} - \tilde{S}_{\text{loc}} \right) \right] \tag{7}$$

in which the mean local steepness S_{loc} is defined as:

$$S_{\text{loc}} = \frac{H_{\text{rms}} \tilde{k}}{2\pi} \quad , \qquad \tilde{k} = \left[\frac{\iint k^{-\frac{1}{2}} E(\sigma, \theta) \, d\sigma \, d\theta}{E_{\text{tot}}} \right]^{-2} . \tag{8}$$

The fitted exponents are $n_1 = 2$ and $n_2 = 6$, corresponding to $S_{\text{loc},1} = 0.05$ and $S_{\text{loc},2} = 0.025$, respectively, with an average value of $\tilde{S}_{\text{loc}} = 0.038$ (see Figure 2(b)). Note that the value of the exponent n_2 was limited to 6 in order to avoid too high a nonlinearity in the expression (6). The shape factor ν is set equal to 500.

The biphase-based expression (6) is combined with the bore-based breaker model of Thornton and Guza (1983), to yield the following formulation, referred to as the biphase breaker model:

$$D_{\text{tot}} = -\frac{3\sqrt{\pi}}{16} \frac{B^3 \bar{f}}{d} \left(\frac{\beta}{\beta_{\text{ref}}} \right)^n H_{\text{rms}}^3 \quad . \tag{9}$$

The source term for depth-induced breaking is compiled in the usual way in SWAN, based on experimental results by Battjes and Beji (1992):

$$S_{\text{brk}} = D_{\text{tot}} \frac{E(\sigma, \theta)}{E_{\text{tot}}} \quad , \tag{10}$$

where E_{tot} is the total variance.

The biphase breaker model (9) contains a total of three calibration parameters, namely the proportionality coefficient B, the reference biphase β_{ref} and the exponent n, given by (7). The latter two parameters have been determined from the Boers (1996) data. The calibration of the parameter B is considered in Section 3.

It should be noted that including a sensitivity to wave steepness in models for depth-induced breaking, as proposed above, has been suggested before by Battjes and Stive (1985). However, in their study, the dependence on wave steepness is considered to be counter-intuitive (higher wave steepness leading to weaker breaking dissipation, and *vice versa*). In the present model, the influence of wave steepness on breaking is included in a more intuitive manner (increasing dissipation with increasing wave steepness, in addition to a primary dependency on nonlinearity), that is also supported by observations (Doering and Bowen 1995; Boers 1996).

b. Model settings

The computations presented here were performed using the SWAN model version 40.72A in stationary mode. For the deep water physics, the combination of wind input S_{in} and saturation-based whitecapping S_{wc} proposed by Van der Westhuysen et al. (2007) was applied. Quadruplet nonlinear interaction S_{nl4} was modelled using the Discrete Interaction Approximation (DIA) of Hasselmann et al. (1985). The shallow water source terms include triad nonlinear interaction S_{nl3} according to Eldeberky (1996) and bottom friction according to Hasselmann et al. (1973), both with their default settings in SWAN. For depth-induced breaking S_{brk}, the subject of this study, both the BJ78 model and the extended model of W09 were considered.

The convergence criteria applied in this study are those proposed by Van der Westhuysen and Van Vledder (2008), based on the so-called curvature-based criteria of Zijlema and Van der Westhuysen (2005).

c. Case selection

This investigation was conducted for a data set of field and laboratory cases which includes both sloping-bed surf zones and finite-depth wave growth situations over near-horizontal topography. These include most cases considered by W09, but additionally feature an extensive data set of Smith (2004) and additional storm conditions for the Amelander Zeegat. The field cases each comprise a single record in time, sampled over one hour unless stated otherwise. The seven laboratory and field situations included in this data set are described below.

1) AMELANDER ZEEGAT

The shallow inter-tidal region behind the Amelander Zeegat in the Dutch Wadden Sea (Figure 1) is the main area of application of this study. Westerly storms provide the opportunity to study finite-depth wave growth over the shallow Wadden Sea interior. A selection of eleven W cases from storms in January and March 2007 was made that feature high wind speeds ($U_{10} = 14$–21 m/s, being approximately uniform in time, both in speed and direction) and

small water depths, yielding small values of the dimensionless depth $gd/U_{10}{}^2$, and high values of the ratio H_{m0}/d. During these storms, twelve wave buoys, arranged in two arrays, were deployed in this region. Here the interior buoys AZB51, AZB61 and AZB62 are considered to evaluate model performance under finite-depth wave growth conditions.

The buoys AZB21, AZB22 and AZB31, located over the ebb tidal shoal during these 2007 storm events, are considered for sloping-bed surf zone conditions. In addition, six cases from two NW storms, recorded in February 2004 and December 2005 are considered. During both of these storms, one or more buoys were located over the ebb tidal shoal, inshore of the surf zone. Water level fields were computed with a calibrated hydrodynamic model. Spatially uniform winds were applied over the model domain, computed as the average of the wind observations at three stations in the Wadden Sea region.

2) Lake Sloten

Lake Sloten in the Netherlands is approximately 4.5×3 km in size. It has a flat, slightly peaty bottom with a characteristic water depth of about 1.7 m. Wind and wave data for this lake have been observed at the station SL29 over the period 1999 to 2007 (Bottema and van Vledder 2009). Based on test cases identified by these authors, a selection of six SW cases featuring high wind speeds ($U_{10} = 15$–23 m/s) was made, yielding small values of the dimensionless depth $gd/U_{10}{}^2$ and high values for the ratio H_{m0}/d. It should be noted that due to the limited fetch available in this small lake, the wave field observed at station SL29 appears to not always be fully depth-limited. Nonetheless, due to the small lake depth, some of the highest values of H_{m0}/d were recorded at this field site.

3) Lake IJssel

Lake IJssel in the Netherlands is approximately 20×60 km in size with a typical depth of about 4–5 m, and has a fairly flat, sandy bottom. Wind and wave data for this lake have been observed at station FL2/FL2n over the period 1997 to 2007 (Bottema and van Vledder 2009). Based on test cases proposed by these authors, a selection of seven SW-W cases was made that feature relatively high wind speeds ($U_{10} = 15$–24 m/s). However, due to the relatively greater water depths, larger values of the dimensionless depth $gd/U_{10}{}^2$ and smaller values of H_{m0}/d are found than for the Amelander Zeegat and Lake Sloten cases. Spatially uniform winds were applied over the model domain, computed as the spatial average of all wind observations in the lake. No currents or water level setup were included.

4) Lake George

Lake George is a shallow lake in Australia. When full, the lake is approximately 20 km long and 10 km wide. It has a relatively horizontal bed of fine-grained silt, with a water depth of approximately 2.5 m. The data set for Lake George considered here was recorded by Young and Verhagen (1996). The selected cases (sampled over 30 minutes) feature a range of values for the dimensionless depth $gd/U_{10}{}^2$ and the ratio H_{m0}/d. However, due to the relatively low wind speeds for the selected cases ($U_{10} = 6$–15 m/s), these dimensionless parameters indicate the least depth limitation of the four field situations featuring finite-depth wave growth (Amelander Zeegat, Lake Sloten, Lake IJssel and Lake George) considered here. Spatially varying wind fields were applied, but water levels were applied as spatially uniform.

5) Boers (1996) flume

The first surf zone data set considered is the laboratory flume experiment by Boers (1996) which features a barred beach. All three wave conditions studied by Boers are included here, namely case 1A, featuring high steepness, case 1B, featuring high, near-breaking steepness and case 1C, featuring low steepness.

6) Battjes and Janssen (1978) flume

The second sloping-bed surf zone data set considered is the laboratory experiment of BJ78. The selected cases feature random, uni-directional waves breaking over a bar-trough beach profile. Two wave conditions are considered here. The first is run 13 of BJ78, representing a situation with mildly breaking waves. The second is run 15 of BJ78, representing a situation with violently breaking waves.

7) Smith (2004) flume

The third surf zone data set considered is the extensive laboratory flume observations presented by Smith (2004). This experiment features waves propagating over a 1:30 plane slope with a variety of incident spectra. The total data set of 31 cases was considered, featuring various degrees of wave steepness, uni-modal and bi-modal spectra and a range of spectral widths.

8) Calibration and validation sets

The total data set of 69 laboratory and field cases was evenly divided into calibration and validation subsets. The division was made such that the two subsets contained representative cases from both the sloping-bed surf zone cases and the finite-depth wave growth cases. The relatively large data sets for the Amelander Zeegat (interior buoys) and Smith (2004) were each divided equally into calibration and validation parts, based on values of the

dimensionless depth gd/U_{10}^2 and offshore wave steepness $S_0 = H_{m0,0}/L_{p,0}$ respectively. Of the smaller data sets, those of Lake Sloten, Lake George and Boers (1996) were selected in their entirety for the calibration subset. In addition to the cases mentioned above, the validation subset featured the data sets of Lake IJssel, the Amelander Zeegat ebb tidal shoal buoys (W and NW storms) and the flume cases of BJ78.

d. Method of analysis

The predictive ability of the investigated model for depth-induced breaking was determined on the basis of scatter index and relative bias scores, which were computed for both the significant wave height H_{m0} and the mean period $T_{m-1,0}$. These measures are defined respectively as

$$\mathrm{SCI}_\Psi = \frac{\sqrt{\frac{1}{N}\sum_{i=1}^{N}\left(\Psi_{\mathrm{SWAN}}^i - \Psi_{\mathrm{obs}}^i\right)^2}}{\frac{1}{N}\sum_{i=1}^{N}\Psi_{\mathrm{obs}}^i} \qquad (11)$$

and

$$\mathrm{Rel.\ bias}_\Psi = \frac{\sum_{i=1}^{N}\left(\Psi_{\mathrm{SWAN}}^i - \Psi_{\mathrm{obs}}^i\right)}{\sum_{i=1}^{N}\Psi_{\mathrm{obs}}^i} \quad , \qquad (12)$$

where Ψ_{obs} is the observed significant wave height $H_{m0,\mathrm{obs}}$ or mean period $T_{m-1,0,\mathrm{obs}}$, and Ψ_{SWAN} is the corresponding modelled value $H_{m0,\mathrm{SWAN}}$ or $T_{m-1,0,\mathrm{SWAN}}$, in a sample of size N. These statistical measures were computed over all cases for a given laboratory or field situation (e.g., Boers (1996) or Amelander Zeegat). Subsequently, these individual scores were averaged to obtain overall scores for, for example, the total validation subset. A simple averaging was applied in order to give all of these data sets equal statistical weight despite the considerable difference in the number of observations contained in each set.

For the calibration of the breaker model, a third statistical measure was used, namely a combined error function ε. This error function is defined in terms of the scatter indices of H_{m0} and $T_{m-1,0}$, as follows:

$$\varepsilon = \frac{1}{2}\left(\mathrm{SCI}_H + \mathrm{SCI}_T\right) \qquad (13)$$

using the definition in (11). As above, this error function was computed over all cases for a given laboratory or field situation. By considering the mean of the error ε over a collection of cases, optimal calibration settings were determined for the total calibration subset, as well as for its sloping-bed surf zone and finite-depth wave growth parts separately.

3. Calibration

The biphase breaker model (9) presented above contains three calibration parameters, namely B, β_{ref} and n. The reference biphase β_{ref} $(= -4\pi/9)$ and the exponent
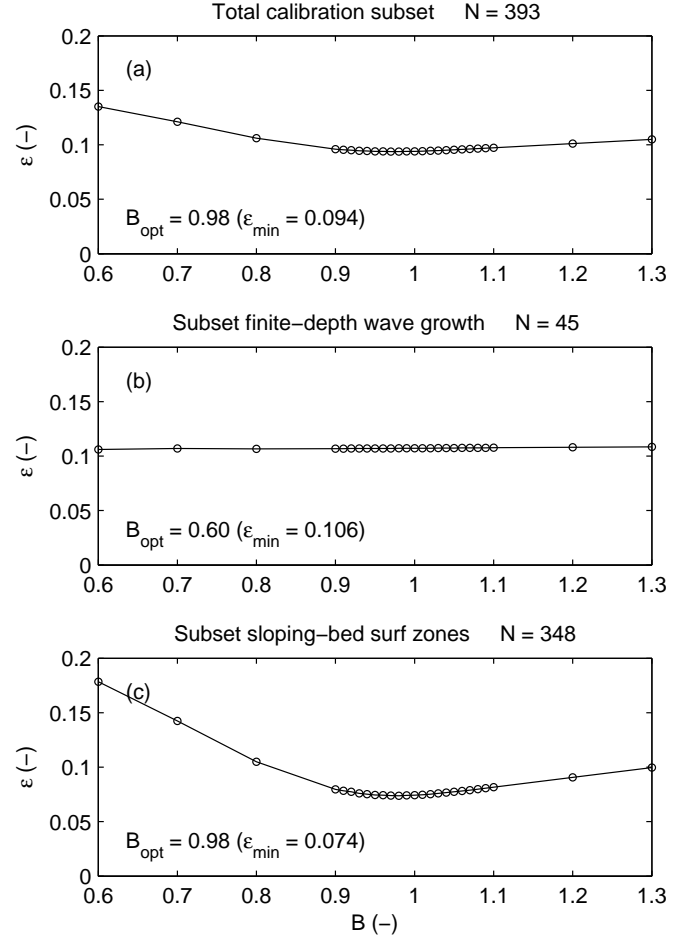
FIG. 3. Variation of the error function ε with the coefficient B in the expression (9), for the calibration subset. Shown are: (a) the total calibration subset, (b) finite-depth wave growth cases and (c) sloping-bed surf zone cases.

n were fitted to the data of Boers (1996), as detailed in Section 2. Subsequently, the coefficient B was calibrated using the total calibration subset. Figure 3 shows that the cases of Boers (1996) and Smith (2004) featured in the surf zone subset display a strong preference for $B = 0.9$ to 1.1, with a minimum error at $B = 0.98$ (Figure 3(c)). For the finite-depth wave growth cases, by contrast, the results are rather insensitive to the choice of B (Figure 3(b)). Figure 3(a) shows that the parameter value $B = 0.98$ therefore also suffices for the total calibration set. This value is higher than that found by W09 (namely $B = 0.90$), being the result of applying the variable exponent n given by (7).

4. Results

The biphase breaker model (9) with the calibration settings $B = 0.98$ and $\beta_{\mathrm{ref}} = -4\pi/9$ is subsequently ap-
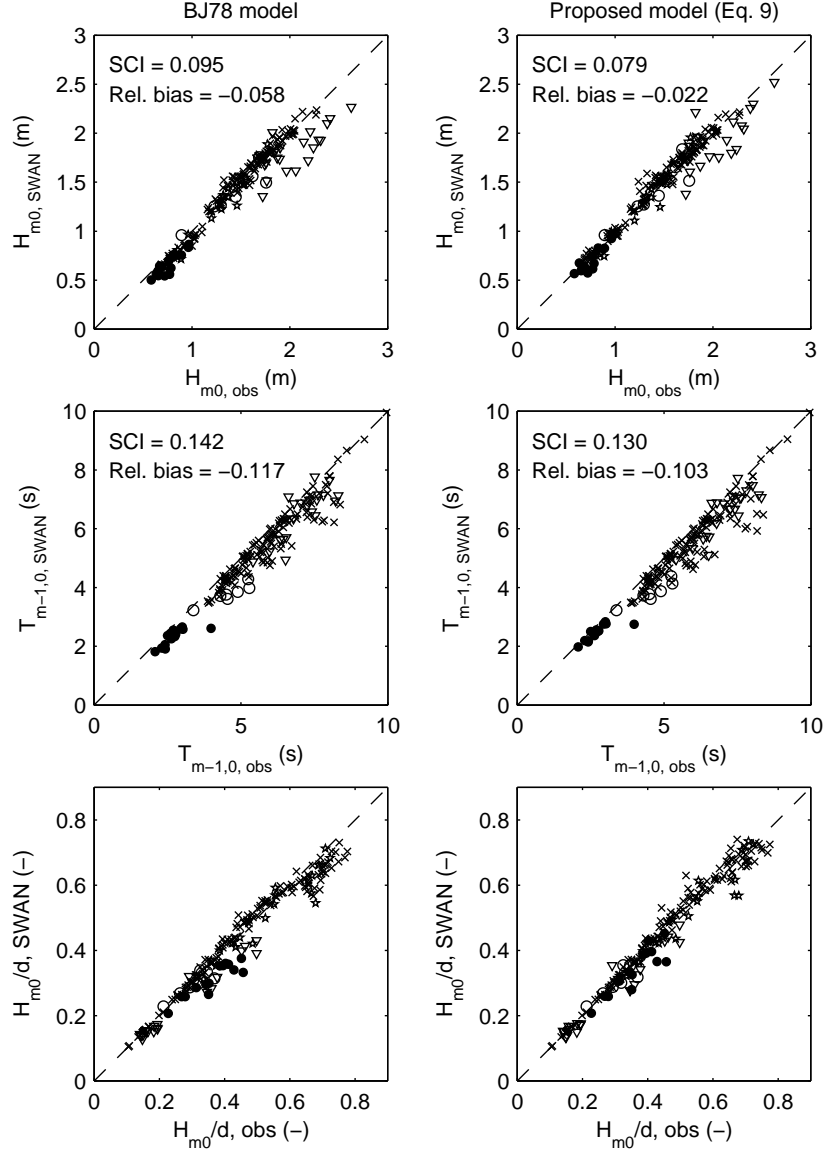
FIG. 4. Scatter plots of model results versus observations of the validation subset for the BJ78 model (with $\gamma_{BJ} = 0.73$, left-hand panels) and with the proposed model (9) (with $B = 0.98$, $\beta_{ref} = -4\pi/9$ and a variable n, right-hand panels). Plotted are results of Amelander Zeegat interior buoys (filled circles), Lake IJssel (open circles), BJ78 (stars), Smith (2004) (crosses) and Amelander Zeegat ebb tidal shoal buoys (inverted triangles). Wave height data of BJ78 and Smith (2004) are scaled up by a factor 10 and 20 respectively for presentation purposes.

plied to the validation subset. Figure 4 shows a scatter plot comparison between model results and observations for the BJ78 model with a constant $\gamma_{BJ} = 0.73$, and the biphase breaker model. It can be seen that the results of the biphase model are generally comparable to those of the BJ78 model, with somewhat better overall statistical scores. As discussed in W09, an important advance made with the biphase model is the improved prediction of finite-depth wave growth conditions, such as those found in the

Amelander Zeegat (interior buoys) and Lake IJssel cases. The underprediction of H_{m0} and H_{m0}/d in the BJ78 model at strong depth limitation (in particular for the Amelander Zeegat) is corrected by the biphase model, which predicts reduced breaking intensity here. However, the mean period $T_{m-1,0}$ remains underpredicted in the Lake IJssel cases and, to some extent, in the Amelander Zeegat. This inaccuracy is related to the inaccurate prediction of the shape of the frequency spectrum, which appears to be too broad
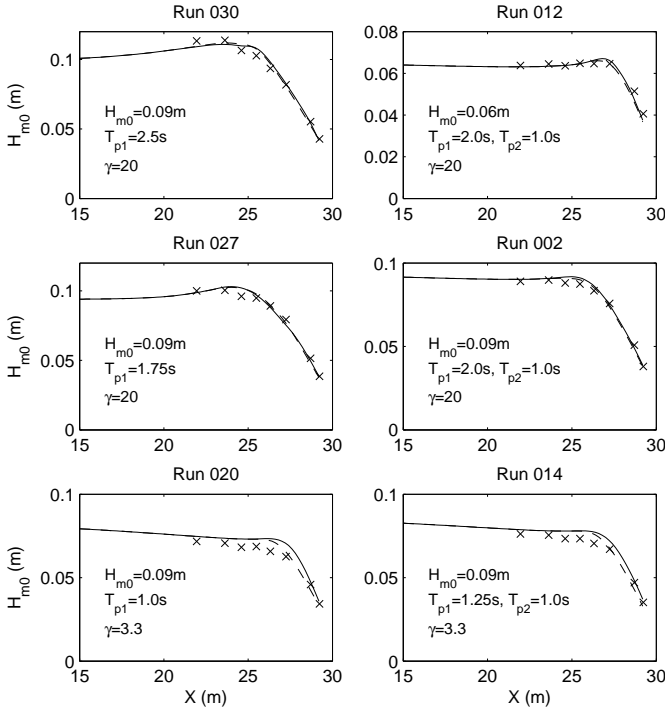
FIG. 5. Simulation results for the Smith (2004) flume experiment, with various wave steepnesses and spectral shapes. Left hand panels: uni-modal spectra, Right-hand panels: bi-modal spectra, with peak periods T_{p1} and T_{p2}. Peak enhancement factor given by γ. Results for proposed model (solid) and BJ78 (dashed), with observations (crosses).

under these shallow water conditions (Van der Westhuysen et al. 2007; Bottema and Van Vledder 2009). This issue was not further pursued here.

For sloping-bed surf zones, the biphase and BJ78 models generally perform comparably. For the laboratory flume data of Smith (2004), which feature a range of wave steepnesses and spectral shapes (including uni-modal and bi-modal spectra), the overall agreement between the two models, and with observations, is good. An exception is found for high values of H_{m0}/d, corresponding to locations close to the shoreline, for which a slight negative bias in the results of the BJ78 model is corrected by the biphase model. However, the biphase model can be seen to over-estimate wave heights compared to observations and the BJ78 model in some instances, as will be discussed below. Compared to these laboratory cases, the field data recorded over the Amelander Zeegat ebb tidal shoal are less well predicted. Both the biphase and BJ78 models tend to under-predict H_{m0} for these cases, although the underprediction is reduced with the biphase model.

Figure 5 shows a representative sample of the wave height evolution along the flume for the Smith (2004) data. The results are arranged in terms of increasing incident wave steepness (rows, from top to bottom), and spectral shape (columns). As suggested by the scatter plot results above, the results of the biphase and BJ78 models agree closely, and reproduce the observations well. Comparison between the results for uni-modal (left-hand column) and bi-modal incident frequency spectra (right-hand column) show no clear sensitivity of model performance to this aspect. By comparison, both models can be seen to perform well for low (top panels) and moderate wave steepness (centre panels), whereas they overestimate H_{m0} for high steepness (bottom panels). In this regard, the biphase model yields somewhat poorer performance than the BJ78 model. This suggests that a somewhat greater dependency of breaking dissipation to local wave steepness than given (7) may be required.

Figure 6 shows an example of the performance of the biphase model for the Amelander Zeegat field case for a south-westerly storm. The conditions shown were recorded on 18/01/2007 at 12:20, and feature $U_{10} = 21.1$ m/s and $U_{dir} = 233°$N, yielding strong finite-depth wave growth conditions in the Wadden Sea interior ($gd/U_{10}{}^2 = 0.039$). Shown are the frequency spectra for the buoys AZB21 /22/31 located inshore of the ebb tidal shoal, and the buoys AZB51/61/62 in the shallow Wadden Sea interior (cf. Figure 1). Despite the south-westly wind, offshore waves refract over the shallow bathymetry offshore of the barrier islands, yielding approximately westerly wave directions here. Hence, wave conditions at AZB21/22/31 are mainly those of offshore waves that break over the ebb tidal shoal. The biphase and BJ78 models produce similar results at these buoy locations, which, at AZB21, agree with the observations. However, at AZB22 and AZB31 both models underestimate the observed spectra to some extent. By comparison, at the buoys AZB51/61/62 in the Wadden Sea interior, the biphase model yields more energetic spectra than the BJ78 model, correcting the underprediction of the observations by the latter. The biphase model can therefore be seen to perform adequately in both the sloping-bed and finite-depth wave growth conditions present in this field case, and to significantly improve model accuracy with respect to the latter.

5. Conclusions and Discussion

The present study aimed to improve the performance of SWAN with respect to the modelling of depth-induced breaking over sloping-bed and finite-depth wave growth situations. To this end, the biphase breaker model of Van der Westhuysen (2009) was extended with a sensitivity to the local mean wave steepness. This model was calibrated and validated for a wide range of cases. Based on the results of this study, the following can be concluded:
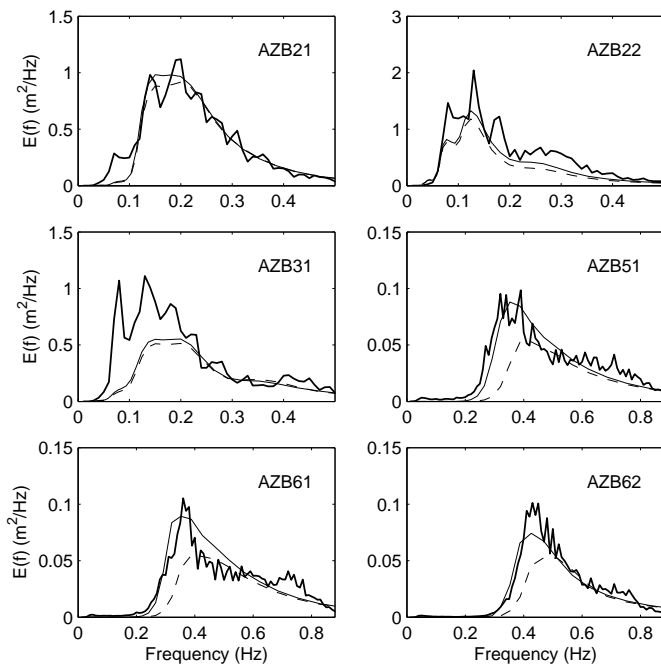
FIG. 6.   Frequency spectra of the Amelander Zeegat storm of 18/01/2007 at 12:20, for buoys in the ebb tidal shoal region (AZB21/22/31) and Wadden Sea interior (AZB51/61/62). Results for proposed model (9) (solid), BJ78 model (dashed) and observations (thick solid).

i. The biphase breaker model of Van der Westhuysen (2009), extended with a sensitivity to the local mean wave steepness, has been shown to perform comparably to the BJ78 model over sloping-bed surf zones under a wide range of conditions. Although the sensitivity of wave breaking to wave steepness has been proposed earlier by Battjes and Stive (1985), the present model includes its influence in an intuitive way (higher steepness yielding greater dissipation), whereas in this earlier study it was not.

ii. For high wave steepnesses in sloping-bed surf zones, the proposed breaker model shows a tendency to produce somewhat greater wave heights than both observations and the BJ78 model. This suggests that a somewhat greater dependency of breaking dissipation on local wave steepness than derived here may be required.

iii. Under finite-depth wave growth conditions, the proposed breaker model produces similar improvements on the BJ78 model to those found by Van der Westhuysen (2009), namely that the underprediction of H_{m0}, H_{m0}/d and $T_{m-1,0}$ under strong depth limitation is corrected.

In closing, the following two discussion points are noted:

i. The inclusion of a sensitivity to the mean wave period in the proposed breaker model (through the Ursell number and the local mean steepness) results in a greater need for the accurate prediction of this parameter. In the surf zone, this implies that a greater emphasis is placed on the acurate modelling of triad nonlinear interaction.

ii. Having corrected the overestimation of depth-induced breaking dissipation under finite-depth wave growth conditions, the focus may be shifted to improving the modelling of the remaining dissipation terms in the shallow water source term balance, namely bottom friction and whitecapping.

References

Apotsos, A., B. Raubenheimer, S. Elgar, and R. T. Guza, 2008: Testing and calibrating parametric wave transformation models on natural beaches. *Coastal Eng.*, **55**, 224–235.

Battjes, J. A. and S. Beji, 1992: Breaking waves propagating over a shoal. *Proc. 23rd Int. Conf. Coastal Eng.*, ASCE, 42–50.

Battjes, J. A. and J. P. F. M. Janssen, 1978: Energy loss and set-up due to breaking of random waves. *Proc. 16th Int. Conf. Coastal Eng.*, ASCE, 569–588.

Battjes, J. A. and M. J. F. Stive, 1985: Calibration and verification of a dissipation model for random breaking waves. *J. Geophys. Res.*, **90 (C5)**, 9159–9167.

Boers, M., 1996: Simulation of a surf zone with a barred beach; Report 1: Wave heights and wave breaking. Communications on Hydraulics and Geotechnical Engineering. Fac. of Civil Engineering, Delft University of Technology, 116 pp.

Booij, N., R. C. Ris, and L. H. Holthuijsen, 1999: A third generation wave model for coastal regions, Part I, Model description and validation. *J. Geophys. Res.*, **104 (C4)**, 7649–7666.

Bottema, M. and D. Beyer, 2002: Evaluation of the SWAN wave model for the Dutch IJsselmeer area. *Proc. 4th Int. Conf. on Ocean Waves (WAVES2001)*, ASCE, 560–569.

Bottema, M., J. P. de Waal, and H. J. Regeling, 2002: Some applications of the Lake IJssel/Lake Sloten wave data set. *Proc. 28th Int. Conf. Coastal Eng.*, ASCE, 413–425.

Bottema, M. and G. P. van Vledder, 2009: A ten-year data set for fetch- and depth-limited wave growth. *Coastal Eng.*, **56**, doi:10.1016/j.coastaleng.2009.01.012.

Bretschneider, C. L., 1958: Revised wave forecasting relationships. *Proc. 6th Conf. Coastal Eng.*, ASCE, 30–67.

De Waal, J. P., 2002: Wave growth limit in shallow water. *Proc. 4th Int. Conf. on Ocean Waves (WAVES2001)*, ASCE, 580–589.

Doering, J. C. and A. J. Bowen, 1995: Parameterization of orbital velocity asymmetries of shoaling and breaking waves using bispectral analysis. *Coastal Eng.*, **26**, 15–33.

Eldeberky, Y., 1996: Nonlinear transformations of wave spectra in the nearshore zone. Ph.D. thesis, Fac. of Civil Engineering, Delft University of Technology, 203 pp.

Gourlay, M. R., 1994: Wave transformation on a coral reef. *Coastal Eng.*, **23**, 17–42.

Groeneweg, J., A. J. van der Westhuysen, G. P. van Vledder, S. Jacobse, J. Lansen, and A. R. van Dongeren, 2008: Wave modelling in a tidal inlet: Performance of SWAN in the Wadden Sea. *Proc. 31th Int. Conf. Coastal Eng.*, ASCE, 411–423.

Hasselmann, K., et al., 1973: *Measurement of wind-wave growth and swell decay during the Joint North Sea Wave Project (JONSWAP)*, Dtsch. Hydrogr. Z. Suppl., Vol. A(8), 12. 95 pp.

Hasselmann, S., K. Hasselmann, J. A. Allender, and T. P. Barnett, 1985: Computations and parameterizations of the nonlinear energy transfer in a gravity-wave spectrum. Part 2: parameterization of the nonlinear transfer for application in wave models. *J. of Phys. Oceanogr.*, **15**, 1378–1391.

Holthuijsen, L. H. and N. Booij, 2006: Experimental wave breaking in SWAN. *Proc. 30th Int. Conf. Coastal Eng.*, ASCE, 392–402.

Massel, S. R. and M. R. Gourlay, 2000: On the modelling of wave breaking and set-up on coral reefs. *Coastal Eng.*, **39**, 1–27.

Nairn, R. B., 1990: Prediction of cross-shore sediment transport and beach profile evolution. Ph.D. thesis, Imperial College, London, 391 pp.

Ruessink, B. G., D. J. R. Walstra, and H. N. Southgate, 2003: Calibration and verification of a parametric wave model on barred beaches. *Coastal Eng.*, **48**, 139–149.

Schäffer, H. A., P. A. Madsen, and R. Deigaard, 1993: A Boussinesq model for waves breaking in shallow water. *Coastal Eng.*, **20**, 185–202.

Smith, J. M., 2004: Shallow-water spectral shapes. *Proc. 29th Int. Conf. Coastal Eng.*, ASCE, 206–217.

Thornton, E. B. and R. T. Guza, 1983: Transformation of wave height distribution. *J. Geophys. Res.*, **88**, 5925–5938.

Van der Westhuysen, A. J., 2009: Modelling of depth-induced wave breaking under finite-depth wave growth conditions. *J. Geophys. Res.*, in press.

Van der Westhuysen, A. J. and G. P. Van Vledder, 2008: Speeding up stationary SWAN computations by dynamic grid point deactivation. *Proc. 31th Int. Conf. Coastal Eng.*, ASCE, 449–461.

Van der Westhuysen, A. J., M. Zijlema, and J. A. Battjes, 2007: Nonlinear saturation-based whitecapping dissipation in SWAN for deep and shallow water. *Coastal Eng.*, **54**, 151–170.

Van Vledder, G. P., J. Groeneweg, and A. J. van der Westhuysen, 2008: Numerical and physical aspects of wave modelling in a tidal inlet. *Proc. 31th Int. Conf. Coastal Eng.*, ASCE, 424–436.

Young, I. R. and A. V. Babanin, 2006: The form of the asymptotic depth-limited wind wave frequency spectrum. *J. Geophys. Res.*, **111 (C06031)**, doi:10.1029/2005JC003398.

Young, I. R. and L. A. Verhagen, 1996: The growth of fetch-limited waves in water of finite depth. Part 1. Total energy and peak frequency. *Coastal Eng.*, **29**, 47–78.

Zijderveld, A. and H. Peters, 2008: Measurement programme Dutch Wadden Sea. *Proc. 31th Int. Conf. Coastal Eng.*, ASCE, 404–410.

Zijlema, M., 2009: Multiscale simulations using unstructured mesh SWAN model for wave hindcasting in the dutch wadden sea. *Proc. Coastal Dynamics 2009.*

Zijlema, M. and A. J. Van der Westhuysen, 2005: On convergence behaviour and numerical accuracy in stationary SWAN simulations of nearshore wind wave spectra. *Coastal Eng.*, **52**, 237–256.